

Ionic Dopant-Free Polymer Alloy Hole Transport Materials for High-Performance Perovskite Solar Cells

Qiang Fu, Xingchen Tang, Hang Liu, Rui Wang, Tingting Liu, Ziang Wu, Han Young Woo, Tong Zhou, Xiangjian Wan, Yongsheng Chen,* and Yongsheng Liu*



Cite This: *J. Am. Chem. Soc.* 2022, 144, 9500–9509



Read Online

ACCESS |



Metrics & More

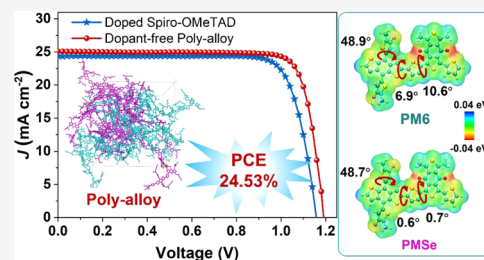


Article Recommendations



Supporting Information

ABSTRACT: The dominated hole transport material (HTM) used in state-of-the-art perovskite solar cells (PSCs) is Spiro-OMeTAD, which needs to be doped to improve its conductivity and mobility. The inevitable instability induced by deliquescent dopants and the necessary oxidation process in air hinders the commercialization of this technology. Here, an alloy strategy using two conjugated polymers with highly similar structures but different crystallinities for dopant-free HTM and high-performance PSCs has been demonstrated. We found that the polymeric packing and crystallinity of a polymer alloy could be regulated finely by blending the polymer PM6 and our developed polymer PMSe, which exhibits a shorter π - π stacking distance due to the improved planarity of the polymer backbone with strong C=O \cdots Se noncovalent interactions. The structure–property relationship of the polymer alloy is investigated by theoretical and experimental analyses. The optimized PSCs using the polymer alloy HTM without any ionic dopants feature an excellent power conversion efficiency of 24.53% and a high open circuit voltage (V_{OC}) of 1.19 V with much improved stability. This efficiency is much higher than that of the control device using doped Spiro-OMeTAD HTM (PCE = 22.54%). Our work provides a very effective strategy to design and construct dopant-free hole transport materials for highly efficient perovskite solar cells and other applications.



INTRODUCTION

Perovskite solar cells (PSCs) have become the leader of the emerging next-generation photovoltaic technologies. The power conversion efficiency (PCE) has reached 25.7%, which is close to monocrystalline silicon solar cells.^{1–9} Hole transport materials (HTMs) play a very important role in high-performance PSCs, and a lot of excellent work has been conducted with small molecules or polymers as HTMs.^{10,11} However, the dominated hole transport material used in the state-of-the-art PSCs is still 2,2',7,7'-tetrakis (*N,N*-di-methoxyphenylamine)-9,9'-spirobifluorene (Spiro-OMeTAD), which needs to be doped with chemical dopants such as tert-butylpyridine (TBP) and lithium bis(trifluoromethanesulfonyl)imide salt (LiTFSI) to achieve efficient hole extraction and sufficient conductivity.^{12,13} The use of deliquescent dopants and the necessary oxidation process of the HTM film in air not only makes the device fabrication more complicated but also has serious negative effects on the stability of perovskite films and devices, which significantly hinder the commercialization of PSCs.^{14,15} Therefore, it has become a challenge and urgent issue by developing dopant-free HTMs to replace the dominated Spiro-OMeTAD and achieve both efficient and stable PSCs.¹⁶ However, the efficiencies of PSCs using dopant-free HTMs reported so far are still much lower than those of the Spiro-

OMeTAD-based device although a lot of efforts have been made in the past decade.^{17–22}

Considering the multiple functional properties of the new generation HTMs, such as hole transport, hydrophobicity, and defect passivation, special functional groups in conjugated polymers or small molecules as HTMs are beneficial for the efficiency and stability of PSCs.^{23,24} The polymer PM6 has abundant Lewis base groups and has been widely studied as a donor material in organic solar cells due to its good hole transport mobility and matched energy levels.²⁵ The concept of polymer alloys has existed for a long time and their principle is to achieve the advantages possessed by two or more others in one material.²⁶ Note that the polymer alloy is a new material with a single-phase structure and it has different physical properties to initial components. The two or more polymers in a polymer alloy must have compatible characteristics. We speculate that the development of polymer alloys with conjugated polymers could cause a lot of excitement in material properties, such as tunable energy levels, enlarged and

Received: April 14, 2022

Published: May 20, 2022



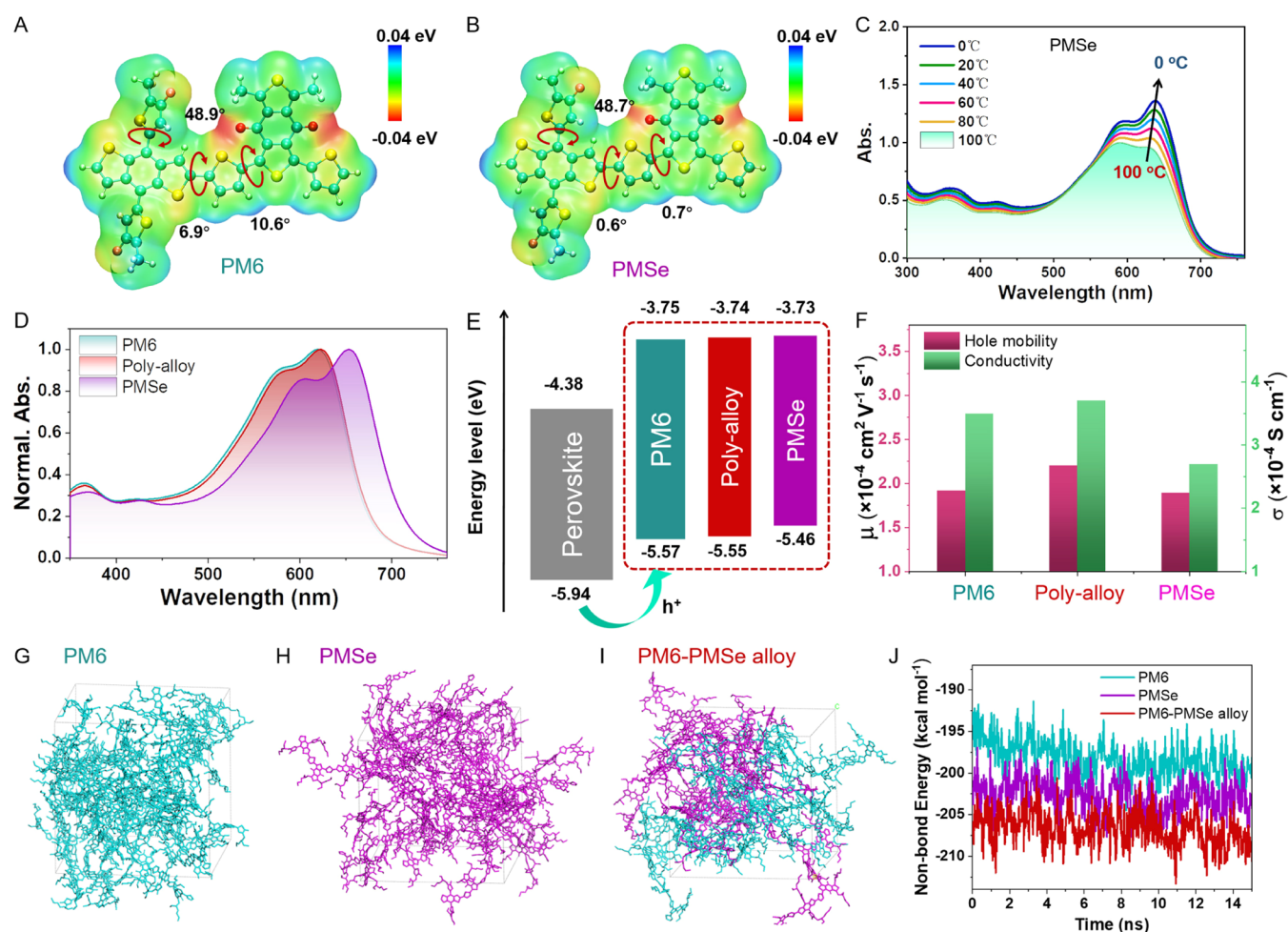


Figure 1. (A, B) Electrostatic potential (ESP) surface of (A) PM6 and (B) PMSe. (C) Absorption spectra of PMSe solution in *o*-xylene at different temperatures. (D) Film absorption spectra of PM6, poly-alloy, and PMSe. (E) Schematic diagram of energy level arrangement. (F) Average hole mobility and conductivity of PM6, poly-alloy, and PMSe films. (G–I) Three configurations of molecular mutual positions from DFT calculations: (G) PM6, (H) PMSe, and (I) poly-alloy. (J) Nonbonding energy between different polymers.

balanced mobility, and optimized film morphology with orientated stacking.^{27,28} However, the conjugated polymer alloys have rarely been studied and have not been used as HTMs in perovskite solar cells.^{11,29}

Here, we developed a PM6 analogue, PMSe, which uses selenophene as a π -bridge and exhibits a rather similar chemical structure. It has been found that the π - π stacking becomes stronger with a smaller distance when replacing the thiophene bridge in PM6 with selenophene. PMSe shows increased crystallinity and a tighter π - π stacking in comparison with PM6 due to the improved planarity of the polymer backbone with stronger C=O \cdots Se noncovalent interactions as demonstrated below. The dopant-free PM6-based device shows an optimized efficiency of 23.60%, much higher than that of the doped spiro-OMeTAD-based device (PCE = 22.54%). More excitingly, after blending with PMSe, a polymer alloy was formed and its molecular packing, crystallinity, and energy levels could be finely regulated. As a result, the optimized polymer alloy (PM6/PMSe) with a mass ratio of 9:1 (we named it poly-alloy) achieves an excellent efficiency of 24.53% and a high V_{OC} of 1.19 V with a low V_{OC} loss (band gap-voltage offset, W_{OC}) of 0.35 V. Furthermore, the poly-alloy-based devices show largely improved stability in comparison with spiro-OMeTAD-based devices under differ-

ent conditions. For example, the device with the poly-alloy HTL could retain 96% of its original efficiency after storage in air (relative humidity, RH = 30 \pm 5%) under dark conditions for 1200 h.

RESULTS AND DISCUSSION

PMSe was synthesized through the Stille coupling polymerization, and a detailed synthesis procedure is shown in Figures S1–S6. The number-average molecular weights (M_n) were determined to be 162.9 and 29.6 kDa with polydispersity indexes (PDIs) of 2.56 and 2.60 for better batches of PM6 and PMSe, respectively (Figures S3–S6). The thermogravimetric analysis (TGA) results showed that the decomposition temperatures at 5% weight loss are 437 and 427 °C for PM6 and PMSe, respectively (Figure S7). Differential scanning calorimetry (DSC) shows that no obvious peak was observed up to 300 °C, indicating no phase transition in these conjugated polymers. Note that the polymers exhibit a good packing structure in a film state due to the self-assembly properties during film preparation (Figure S8). The electronic and geometric properties of PM6 and PMSe were investigated by density functional theory (DFT) calculations. As shown in Figures 1A,B and S9 and S10, PM6 exhibits large dihedral angles of 6.9 and 10.6° between thiophene and two adjacent

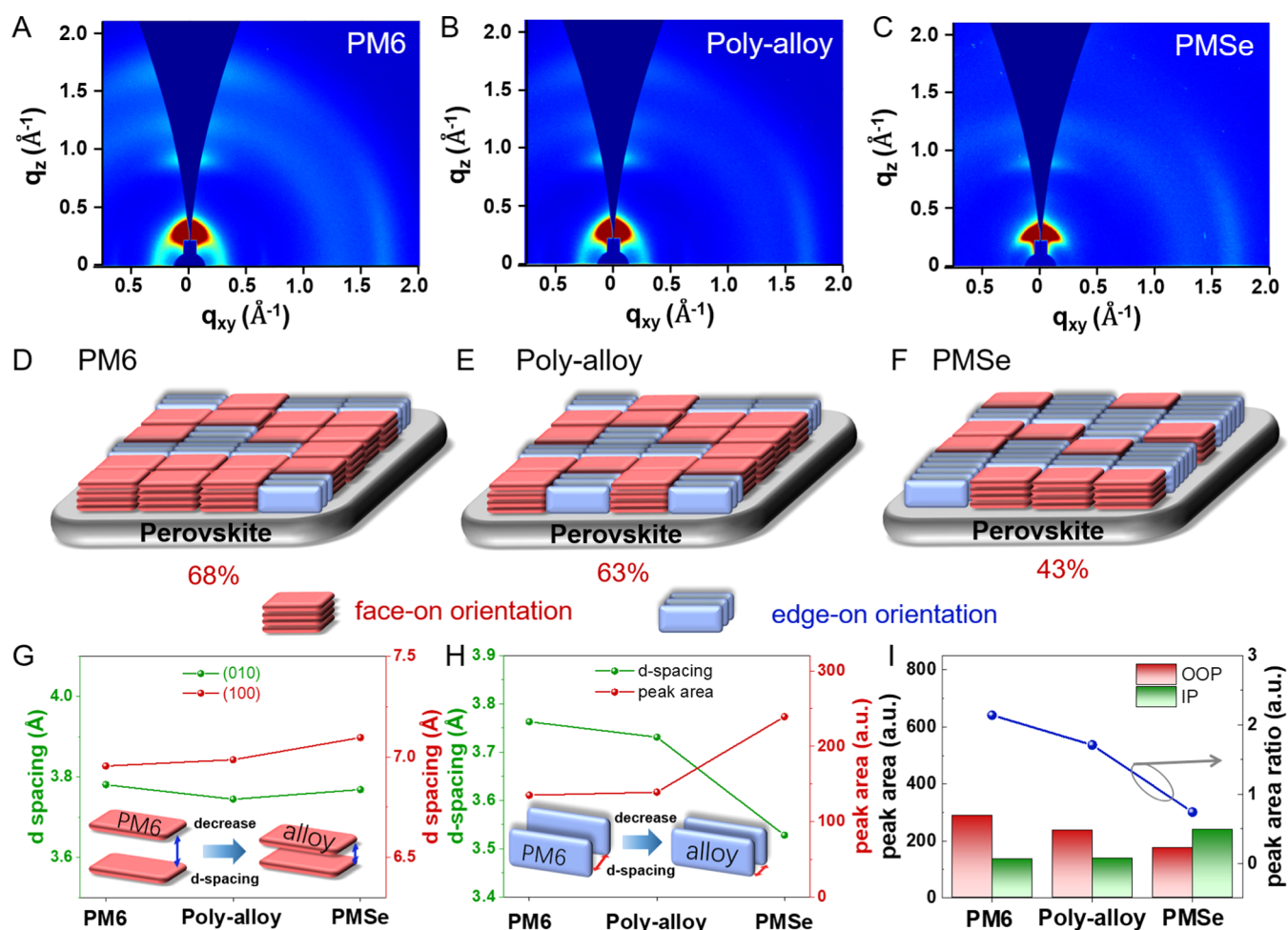


Figure 2. (A–C) GIWAXS scattering patterns of PM6, poly-alloy, and PMSe films. (D–F) Schematic illustration of the orientation distribution in PM6, poly-alloy, and PMSe films. Notes: The face-on/edge-on ratio in this figure is estimated from the integral area of π - π stacking diffraction along the q_{xy} axis and q_z axis. (G) d -Spacing of π - π stacking diffraction of out-of-plane (OOP). (H) d -Spacing of π - π stacking diffraction in the in-plane direction for PM6, poly-alloy, and PMSe. (I) Peak area and peak area ratio of π - π stacking diffraction in out-of-plane and in-plane directions for PM6, poly-alloy, and PMSe.

BDTT and BDD units, respectively. The related dihedral angles in PMSe were decreased to 0.6 and 0.7°, suggesting the enhanced skeleton planarity, which could be attributed to the large orbital overlap between Se in selenophene and O in the carbonyl group due to the large atomic radius of Se. These calculated results are consistent with experimental results for similar compounds in the literature.³⁰

Electrostatic surface potential (ESP) maps revealed that the negative electrostatic potential (red color) is mainly localized in the O of the carbonyl group, which could passivate the undercoordinated Pb²⁺ on the perovskite surface,³¹ consistent with the X-ray photoelectron spectroscopy (XPS) data discussed below. The temperature-dependent ultraviolet–visible absorption (UV–vis) analyses in Figures 1C and S11 revealed that all of the polymer systems have similar temperature-dependent aggregation properties. The enhanced temperature-dependent aggregation property of PMSe indicates that PMSe has a better π - π stacking structure in the film (Figure S12) in comparison with PM6.³²

To verify the formation of polymer alloys for the blended PM6/PMSe film, the UV–vis absorption spectra of polymer films with different weight ratios of PM6/PMSe were investigated. As shown in Figures 1D and S13, the PMSe film displays obvious red-shifted absorption due to the stronger

electron-donating ability of selenophene units, as well as improved film crystallinity in comparison with PM6.³³ The UV–vis spectra of the blended PM6/PMSe films with different weight ratios have two similar absorption peaks, which are red-shifted with increasing of PMSe ratio, indicating that the two polymers have formed a polymer alloy instead of a simple mechanical blending.³⁴ Moreover, the polymer PBDB-T with the same molecular skeleton can also form an alloy structure with PMSe (Figure S14). To further prove our alloy polymer strategy, we selected three well-studied polymers (PTB7-Th, PTQ-10, P3HT), which have different molecular skeletons from PMSe. By blending these polymers with PMSe (w/w = 5:5), the characteristic absorption peak of these polymers and PMSe appear simultaneously (Figure S15), indicating that these polymers cannot form the polymer alloy with PMSe. The highest occupied molecular orbital (HOMO) energy levels were determined from cyclic voltammetry (CV) curves of the HTMs in films (Figure S16 and Table S1). The lowest unoccupied molecular orbital (LUMO) energy levels were calculated by subtracting the E_g^{opt} from the HOMO level. The lack of a new oxidation peak and the slightly increased HOMO levels with increasing of PMSe content (Figures S16 and 1E) further indicate that the polymer alloys were formed by blending PM6 and PMSe with different weight ratios.²⁷ We

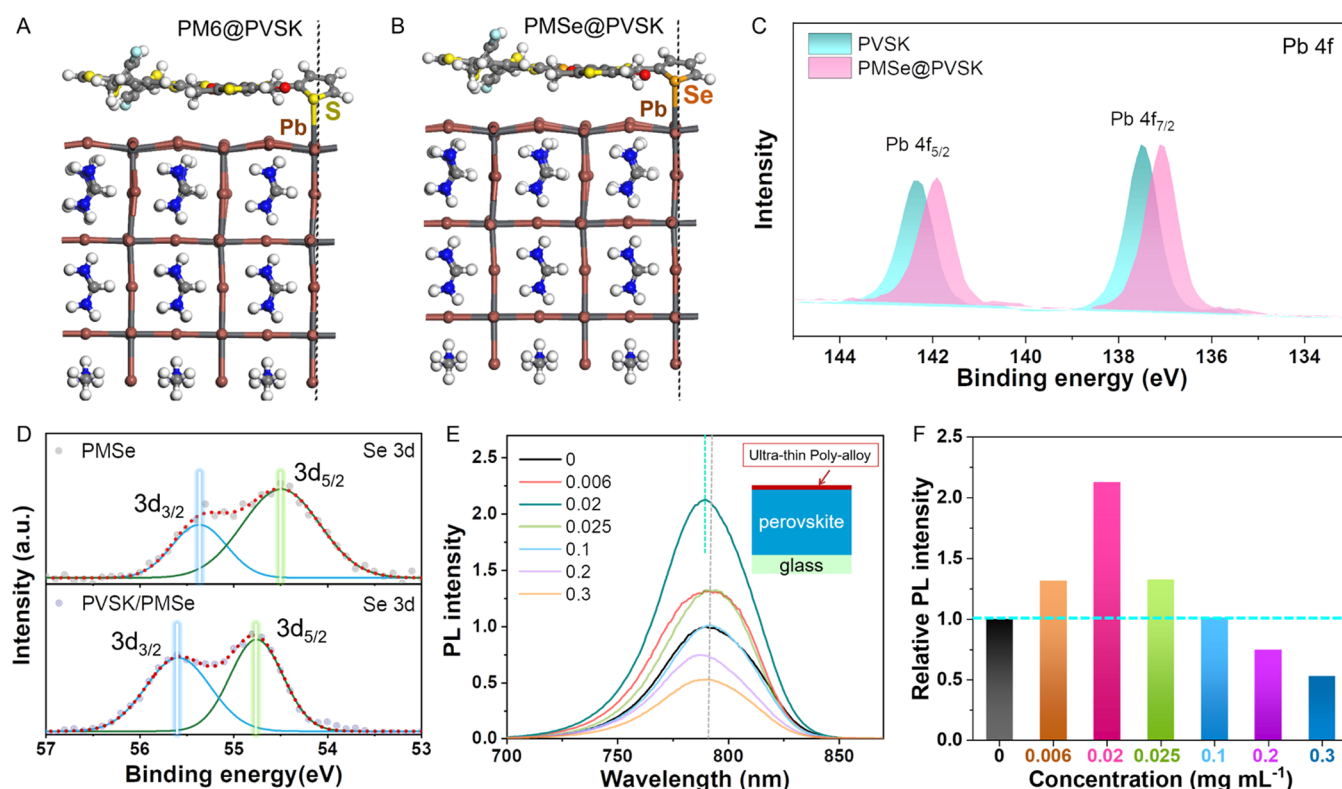


Figure 3. (A, B) Theoretically modeled stacking patterns of PM6 (A) and PMSe (B) on top of a perovskite (PVSK) surface. (C) Pb 4f peaks of the pristine perovskite film, and the perovskite film coated with the PMSe thin layer. (D) XPS of Se 3d peaks of the pristine PMSe film and PMSe-capped perovskite film. (E) Steady-state photoluminescence (PL) spectra of the perovskite film capped with an ultrathin poly-alloy HTL layer with different thicknesses. Poly-alloy HTL was spin-coated on the perovskite film at 1000 rpm using different concentrations (from 0 to 0.3 mg mL⁻¹ in *o*-xylene solution). The PL intensity was based on the peak PL of the pristine perovskite film, which was normalized to 1. (F) Relative peak PL intensity of poly-alloy-capped perovskite films versus thickness of poly-alloy extracted from the corresponding PL curves in panel (E).

named the polymer alloy with a weight ratio of 9:1 (PM6/PMSe) as poly-alloy. The average optimized hole mobilities of the pristine HTMs measured by space-charge-limited current (SCLC) measurements (Figures 1F and S17) are 1.92×10^{-4} , 2.20×10^{-4} , and 1.89×10^{-4} cm² V⁻¹ s⁻¹ for PM6, poly-alloy, and PMSe, respectively. The average conductivities of the pristine HTMs are 3.5×10^{-4} , 3.7×10^{-4} , and 2.7×10^{-4} S cm⁻¹ for PM6, poly-alloy, and PMSe, respectively (Figures 1F and S18). The slightly enlarged hole mobility and conductivity in poly-alloys can be explained by denser polymer backbone packing through noncovalent intermolecular and intramolecular interactions induced by Se atoms, which exhibit a larger atom radius than a S atom, resulting in the slightly enhanced J_{SC} and FF values for poly-alloy-based PSCs discussed below. The trap-state densities of different HTM-coated perovskite films were estimated by the SCLC method with a device structure of ITO/PEDOT:PSS/perovskite/HTM/Ag. The corresponding average trap-state densities of perovskite films were determined to be 1.1×10^{16} cm⁻³ with PM6 HTM, 8.5×10^{15} cm⁻³ with poly-alloy HTM, and 5.6×10^{15} cm⁻³ with PMSe HTM (Figure S19). The gradually decreasing trap-state density for these HTM-coated perovskite films indicated that there is a better surface passivation effect of PMSe.³⁵ The steady-state photoluminescence (PL) spectra show that the PL intensity of the perovskite film was quenched to 12.8% of its initial intensity after coating a PM6 layer. The original PL intensity was quenched to 7.5 and 3.4% for the poly-alloy and PMSe-capped perovskite, respectively (Figure S20). The results suggest that the poly-alloy and PMSe could extract

hole carriers more efficiently, which could be attributed to the better surface defect passivation as well as the larger binding energy between PMSe and the perovskite film discussed below.

Molecular dynamics simulations were performed to further verify the formation of a polymer alloy structure. Three nonbonding interaction models and the corresponding calculated nonbonding energies between various polymers are shown in Figure 1G–J. The lower nonbonding energy of PMSe in comparison with PM6 indicates that a larger interpolymer interaction occurs between PMSe, leading to stronger aggregation of PMSe.³⁰ Importantly, stronger nonbonding energy was observed between PM6 and PMSe, further verifying that PM6 and PMSe could form a polymer alloy due to their highly similar polymer structure and stronger interpolymer interactions.³⁶

The crystallization and aggregation of PM6/PMSe polymer films with different weight ratios were investigated by grazing incidence wide-angle X-ray scattering (GIWAXS) (Figures 2A–C and S21). The pristine PM6 film has a dominant π – π stacking diffraction peak at $q = 1.66$ Å⁻¹, corresponding to a d -spacing of 3.78 Å. The major polymer packing in the out-of-plane direction suggests the formation of a typical predominant face-on orientation with an out-of-plane π – π stacking ratio of ~68%, which was estimated from the integral area of π – π stacking diffraction along the q_{xy} axis and q_z axis. The poly-alloy film also has a predominant face-on orientation (~63% ratio) and a π – π stacking diffraction peak at $q = 1.67$ Å⁻¹ with a decreased d -spacing of 3.75 Å, indicating a tighter π – π stacking due to a more flat skeleton of PMSe and formation of

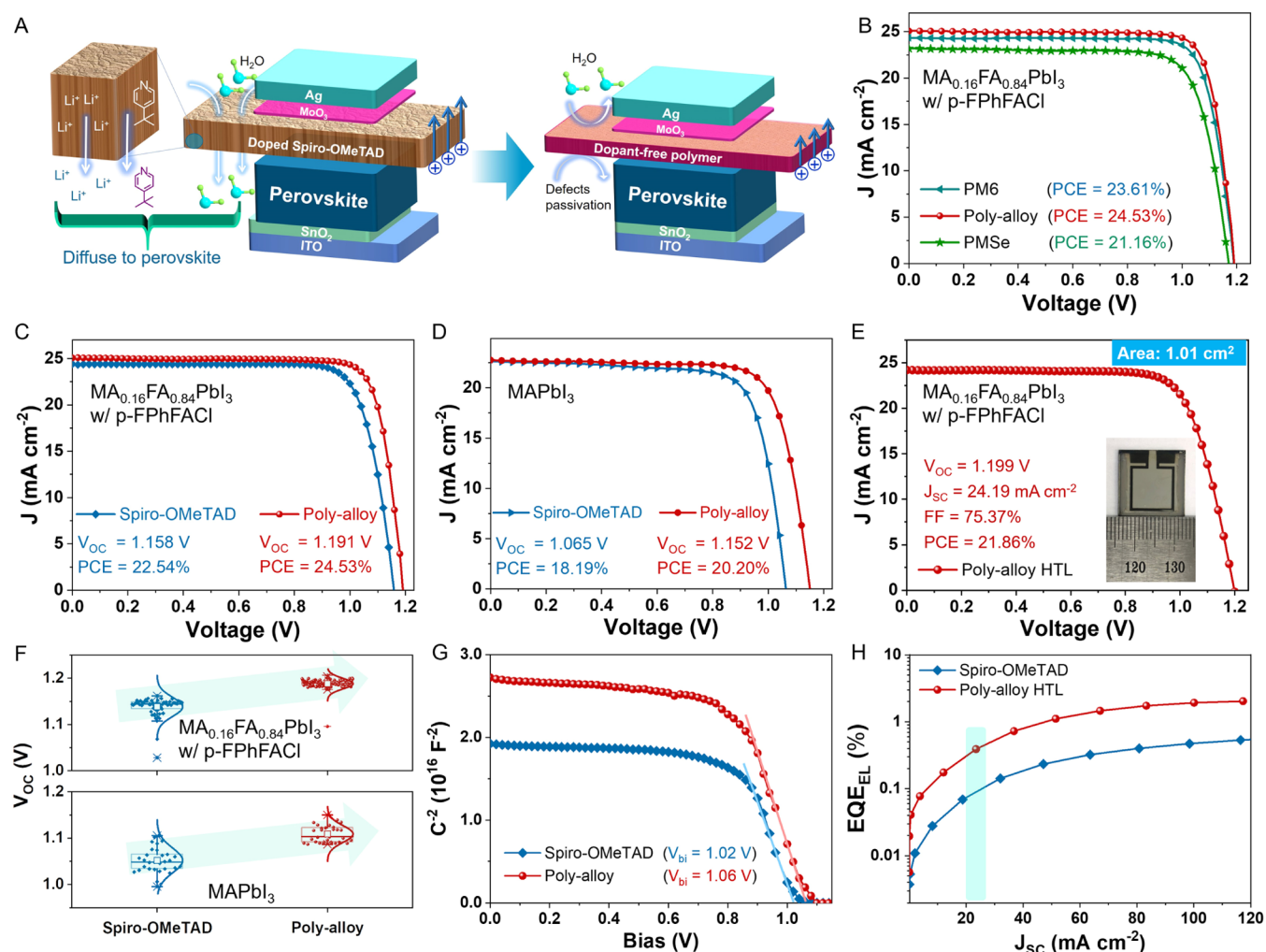


Figure 4. (A) Device structures of perovskite solar cells illustrate the disadvantages of the device based on ionic-doped spiro-OMeTAD and the advantages of the device based on the ionic dopant-free polymer HTL. (B) J - V curves of the PSCs based on different polymer HTMs with the perovskite composition: p-FPhFA-incorporated MA_{0.16}FA_{0.84}PbI₃ perovskite. (C, D) J - V curves of the PSCs based on the dopant-free poly-alloy HTL and doped Spiro-OMeTAD with different perovskite compositions: (C) p-FPhFA-incorporated MA_{0.16}FA_{0.84}PbI₃ perovskite and (D) MAPbI₃. (E) J - V curve of a large-area PSC (area: 1.01 cm²) based on the dopant-free poly-alloy HTL. Inset is the picture of a large-area PSC. (F) Statistical V_{oc} data of the corresponding devices. (G) Mott-Schottky plots of the corresponding devices. (H) EQE_{EL} as a function of the injection current density for poly-alloy HTLs and doped Spiro-OMeTAD-based PSCs when operating as a light-emitting diode (LED).

polymer alloys (Figure 2G,H). The diffraction profiles of the polymer alloy with a weight ratio of 5:5 and pristine PMSe films are quite similar (Figures 2C and S21), but their π - π stacking reflection is less oriented in comparison with PM6 and poly-alloy, suggesting a more random orientation,³⁷ as illustrated in Figure 2D-F. The peak area ratios of the π - π stacking reflection in out-of-plane to that in in-plane for PM6 and poly-alloy are ~ 2.1 and ~ 1.7 , respectively, while the values of polymer alloys with a weight ratio of 5:5 and pristine PMSe are both close to 0.7 (Figures 2H,I and S21), indicating that the PM6 and poly-alloy films exhibit better π - π stacking with more paralleled orientation with respect to the substrate. This stacking characteristic could reduce the surface disorder at the interface between the perovskite and polymer HTL, resulting in efficient hole transport.³⁸

DFT calculations were further conducted to study the interaction between the HTM and perovskite surface. Here, two repeat segments of polymeric HTMs were positioned on top of a perovskite crystal model and optimized with subsequent constraints. As shown in Figures 3A,B and S22,

with a rigid and bulk conjugated skeleton, the two polymeric HTMs interact tightly with the perovskite surface. The selenium atoms in PMSe could easily interact with under-coordinated Pb²⁺ at the perovskite surface due to its larger atomic radius than that of sulfur as characterized by a calculated bond length of 3.68 Å. The binding energy between the PMSe segment and perovskite layer (Figure 3B) was calculated to be -5.3 kcal mol⁻¹, which is significantly larger than that between PM6 and perovskites (-4.0 kcal mol⁻¹) (Figure 3A). The larger binding energy indicates the tighter packing between PMSe and the perovskite film, which will lead to a larger orbital overlap of perovskites and PMSe in the interface, resulting in efficient hole extraction.²⁰ We speculate that the more rigid and planar structure of PMSe as well as stronger Se...Pb interactions should be responsible for the tighter packing between PMSe and the perovskite film. The Fourier transform infrared (FTIR) spectra in Figure S23 show that the pristine PMSe exhibits a stretching vibration of C=O around 1638 cm⁻¹, which is downshifted to 1622 cm⁻¹ after spin-coated on top of the perovskite film, suggesting a strong

interaction between C=O in PMSe and undercoordinated Pb^{2+} in the perovskite surface. PM6 also exhibits similar interaction with the perovskite surface (Figure S23). To better understand the interactions between the perovskite surface and polymer HTMs, XPS characterizations were performed (Figures 3C,D and S24). The Pb 4f for the PMSe-capped perovskite film shows two main peaks at 137.1 and 141.9 eV, corresponding to Pb 4f_{7/2} and Pb 4f_{5/2}, respectively, whereas the Pb 4f peaks are located at 137.5 and 142.3 eV for the pristine perovskite film (Figure 3C). The shifted Pb 4f peaks to higher binding energies in PMSe-capped perovskite films could be ascribed to the Se...Pb and C=O...Pb interactions between Se and carbonyl in PMSe and undercoordinated Pb^{2+} in the perovskite surface. The Se 3d peaks for PMSe-coated perovskite films are located at 54.8 and 55.6 eV, corresponding to Se 3d_{5/2} and Se 3d_{3/2}, respectively, whereas the two peaks are located at 54.5 and 55.3 eV for the pristine PMSe film (Figure 3D), indicating a direct interaction between selenium in PMSe and the perovskite surface. The peaks from Pb 4f, O 1s, and S 2p of PM6-capped perovskites also have similar shifts (Figure S24). These results revealed that PM6 and PMSe could bind the exposed and undercoordinated Pb^{2+} defects by acting as a Lewis base, thereby effectively passivating the trap on the perovskite surface.²³ Thickness-dependent steady-state PL was conducted to study the surface passivation and hole extraction properties of poly-alloy (Figures 3E,F and S25). The passivation effect of poly-alloy on the perovskite surface was confirmed by steady-state photoluminescence (PL) measurements, which show increased PL intensity for the perovskite film after depositing an ultrathin (less than 0.1 mg mL⁻¹ in *o*-xylene for 1000 rpm) poly-alloy film, implying the passivated surface defect and suppressed nonradiative recombination loss.³⁹ Note that the PL intensity of poly-alloy-capped perovskite films was decreased with the increase of poly-alloy film thickness with a poly-alloy concentration larger than 0.1 mg mL⁻¹, indicating that the thicker poly-alloy film plays a role not only in perovskite surface passivation but also in hole extraction and transport.

We have fabricated the solar cells with the n-i-p device architecture of ITO/SnO₂/perovskite/HTMs/MoO₃/Ag using poly-alloy as the dopant-free HTM (Figure S26). Figure 4A illustrates the disadvantage of the device based on ionic-doped spiro-OMeTAD and the advantage of devices based on the ionic dopant-free polymer HTL, which could not only prevent the moisture invasion and passivate the surface defects but also extract and transport the hole carrier efficiently, as verified by the results above. A very thin layer of MoO₃, which has been widely used in perovskite solar cells and organic solar cells, was used here to form a high work function contact buffer for efficient hole injection/extraction as well as protect the perovskite underneath from damage caused by Ag deposition.^{22,40,41} Note that the MoO₃ layer may also promote hole extraction and transport in terms of remote interfacial doping.⁴² The devices using polymers with different solvents and molecular weights were also investigated, and the results (Table S2) show that the molecular weight has an obvious impact on the performance. PMSe with a smaller molecular weight shows a better device performance, which could be ascribed to the less efficient contact between the perovskite layer and HTL owing to the stronger crystallinity of PMSe with a larger molecular weight. Therefore, we choose the best-performance batch with a lower molecular weight for the poly-alloy HTL. Figure 4B shows the *J*-*V* curves of PSCs with a p-

FPhFA-incorporated MA_{0.16}FA_{0.84}PbI₃ perovskite using our poly-alloy and other HTMs. These HTMs contribute to the best device with a low precursor concentration of 5–6 mg mL⁻¹, which is much lower than that of spiro-OMeTAD (~80 mg mL⁻¹), indicating their great potential to improve the economic feasibility of PSCs. Note that PM6 and poly-alloy HTMs processed by *o*-xylene have better device performance than chloroform, whereas PMSe is more effective when processed by chloroform. The optimized thicknesses of PM6, poly-alloy, and PMSe HTL are 36.4, 33.7, and 27.7 nm measured by atomic force microscopy (AFM), respectively (Figure S27). The detailed *J*-*V* curves and efficiency statistics upon systematical optimizations are shown in Figures S28–S30 and Table S2–S8. The PSC using dopant-free PM6 as the HTM displays a peak PCE of 23.60%, coupled with a *J*_{SC} of 24.34 mA cm⁻², a *V*_{OC} of 1.19 V, and an *FF* of 81.52% (Figure 4B and Table S3). By contrast, the dopant-free PMSe-based perovskite device shows a slightly lower *V*_{OC} of 1.17 V, a *J*_{SC} of 23.19 mA cm⁻², and an *FF* of 77.93%, achieving a relatively lower PCE of 21.16%, which could be ascribed to the more random stacking orientation, lower hole mobility and conductivity, and upshifted HOMO level of PMSe films discussed above. The optimized device based on the poly-alloy HTM exhibits a *V*_{OC} of 1.19 V, a high *J*_{SC} of 25.07 mA cm⁻², and a notable *FF* of 82.17%, leading to a champion efficiency of 24.53%. This PCE was much higher than the device using doped Spiro-OMeTAD as the HTM (PCE = 22.54%) (Figure 4C and Table S9). The slightly lower *V*_{OC} of the device based on PMSe in comparison with PM6 could be ascribed to the slightly higher HOMO levels as discussed above, which may increase the energy loss when the hole is transported from the perovskite to the HTM. As expected, the *V*_{OC} of poly-alloy-based devices was maintained due to the almost unchanged HOMO levels compared to that of PM6. The overall improved PCE of poly-alloy-based devices should be ascribed to a synergistic effect of matched energy levels, suitable hole mobility, and efficient surface defect passivation of the poly-alloy HTM. The morphology of HTL could also have a large effect on the device performance due to different crystallinities of the polymers. With the nonhalogen solvent, *o*-xylene, as a solvent to process PM6 and the poly-alloy film, the devices show much better photovoltaic performance than that of the device using chloroform as a solvent (Table S3). While PMSe processed with the *o*-xylene solvent shows inferior performance in comparison with chloroform due to its relatively high crystallinity. Note that the PSCs based on dopant-free poly-alloy HTM exhibit a smaller hysteresis than the doped Spiro-OMeTAD-based device (Figure S31 and Table S10) thanks to the more efficient charge collection and surface passivation. A stabilized PCE of 23.30% was achieved for the device based on the poly-alloy HTM by holding the bias of 1.02 V at the max power point, whereas the PM6-based device exhibits a PCE of 22.66% at the bias of 1.00 V (Figure S32). The integrated *J*_{SC} values from external quantum efficiency (EQE) spectra (Figure S33 and Table S9) are 24.13 and 24.43 mA cm⁻² for Spiro-OMeTAD and poly-alloy HTM-based devices, respectively, matched well with the values measured from the *J*-*V* curves (<3% discrepancy). The perovskite devices based on the poly-alloy HTM (Figure S34 and Table S9) show good reproducibility with an average PCE of 23.66 ± 0.33% for 100 individual devices, which has 12.1% improvement in comparison with the devices based on doped Spiro-OMeTAD (PCE_{average} = 21.11 ± 0.67%). Moreover, we further show the

advantage of poly-alloy-based PSCs by constructing large-area devices with an active area of 1.01 cm². Benefiting from the good material properties and film quality of poly-alloy HTLs, an excellent efficiency of 21.86% was achieved, along with an *FF* of 75.37%, a *V*_{OC} of 1.199 V, and a *J*_{SC} of 24.19 mA cm⁻² (Figures 4E and S35 and Table S11).

The effectiveness of the poly-alloy HTL has been validated in more perovskite systems. For a MAPbI₃ perovskite system (Figure 4D), a champion PCE of up to 20.19% (average PCE: 18.92±0.51%, Figure S36 and Table S12) was achieved, with a *V*_{OC} of 1.15 V, a *J*_{SC} of 22.77 mA cm⁻², and an *FF* of 77.13%. This efficiency has ~11% improvement in comparison with the devices based on doped Spiro-OMeTAD (PCE = 18.19%). The best-performing MA_{0.16}FA_{0.84}PbI₃-based 3D PSC with poly-alloy HTL (Figures S37 and S38 and Table S13) exhibits a *V*_{OC} value of 1.17 V, a *J*_{SC} of 24.49 mA cm⁻², and an *FF* of 81.19%, yielding a high PCE of 23.18%. For comparison, the control device with the doped Spiro-OMeTAD HTL shows a lower PCE of 21.40%. To further verify the effectiveness of our alloy strategy, we blend the polymers PBDB-T and PMSe to form the polymer alloy HTL (w/w, PBDB-T/PMSe = 9:1), and an efficiency of over 23% has been achieved (Figures S39 and S40 and Table S14). These results indicate that our molecular design and alloy regulation strategies have a promising prospect of generality and extended applications.

We note that the biggest contribution to the improved performance with the poly-alloy HTL comes from the increase in *V*_{OC} (Figure 4F). The champion *V*_{OC} of 1.21 V is achieved with a low band gap-voltage offset of 0.33 V for p-FPhFA-incorporated MA_{0.16}FA_{0.84}PbI₃ perovskite devices using poly-alloy as the HTL (Table S14) (average *E*_g = 1.54 eV, as shown in Figure S41). The improved *V*_{OC} was further validated by the Mott–Schottky analysis, which can be used to evaluate the effect of the poly-alloy HTL on the built-in potential (*V*_{bi}) of the device. As shown in Figure 4G, the poly-alloy HTL-based device exhibits a larger *V*_{bi} (1.06 V) than that of the Spiro-OMeTAD-based device (*V*_{bi} = 1.02 V), indicating that the photogenerated carrier in the poly-alloy-based device could be separated more efficiently and resulted in a large output voltage.⁴³ To evaluate the nonradiative recombination photovoltage loss ($\Delta V_{OC,nr}$), the external electroluminescence yield (EQE_{EL}) versus injection current was measured by operating the PSC device as a light-emitting diode (LED) in forward-voltage bias (Figures S42 and 4H).⁴⁴ The nonradiative recombination voltage loss ($\Delta V_{OC,nr}$) in principle can be quantified from the measured EQE_{EL} using the following equation: $\Delta V_{OC,nr} = V_{OC,rad} - V_{OC} = - (kT/q) \ln EQE_{EL}$.^{45,46} As shown in Figure 4H, the poly-alloy HTL-based device exhibited an EQE_{EL} of up to 0.44% at current injection equivalent to the *J*_{SC}, corresponding to a $\Delta V_{OC,nr}$ of 140 mV, lower than that of the control device using doped Spiro-OMeTAD (176 mV). These results indicate that the poly-alloy HTL can effectively eliminate nonradiative recombination pathways at the perovskite/HTL interface, resulting in increased *V*_{OC}.⁴⁶

The charge transfer dynamics in the interface between the perovskite and HTM films was evaluated by steady-state photoluminescence (PL) and time-resolved PL (TRPL) measurements. Figure S43 shows that the PL quenching efficiencies of Spiro-OMeTAD and poly-alloy HTL-capped perovskite films are 84.2 and 92.5%, respectively, indicating better hole extraction capability of poly-alloy. The TRPL curves (Figure S43) show that the pristine perovskite film

exhibits a longer bulk charge carrier lifetime (τ_2) (Table S15) of 2067 ns. In the case of HTM-capped perovskite films, PL lifetimes were reduced to 93 and 21 ns for the doped Spiro-OMeTAD and dopant-free poly-alloy coated films, respectively. The much decreased PL intensity and shortened PL lifetime could be attributed to a better charge extraction capability of poly-alloy in comparison with doped Spiro-OMeTAD. In addition, the charge transport resistance of the poly-alloy-based device was 186 Ω measured by impedance spectra (Figure S44), which is much lower than that of the device based on Spiro-OMeTAD (531 Ω), suggesting significantly suppressed charge recombination at the interface between the perovskite and polymer HTMs due to the efficient defect passivation of the perovskite surface by poly-alloy. The result was further verified by the light intensity dependence of *J*_{SC} and *V*_{OC} (Figure S45) as well as transient photocurrent (TPC) and transient photovoltage (TPV) measurements (Figure S46).

We probed the water wetting behavior of the pure poly-alloy film and doped Spiro-OMeTAD film-coated perovskites using water contact angle measurements. As shown in Figure S47, the poly-alloy-capped film showed a large water contact angle of 108.8° and a retained contact angle of 101.0° after 3 min, whereas the Spiro-OMeTAD-capped film shows a small water contact angle of 81.0° and the contact angle was decreased to 60.6° after 3 min. Importantly, we found that the XRD data and photos of poly-alloy-capped perovskite films remain unchanged (Figures S48 and S49) after being stored for 7 days in air with high humidity (RH = ~80%). These results suggest that the poly-alloy film has better hydrophobicity and water resistance than that of doped Spiro-OMeTAD due to the dense film morphology of poly-alloy, which could fully cover the perovskite surface (Figures S50 and S51). The long-term stability of the unencapsulated devices has been tested under different conditions. The poly-alloy HTL device retained 93% of its original PCE after being stored in the N₂-filled glovebox for 3000 h, showing great storage stability (Figure S52). The ambient stability results (Figure S53) show that the cells with the poly-alloy HTL retained ~96% of their initial efficiency after 1200 h, whereas the control cell with a Spiro-OMeTAD HTL dropped to ~64% of its original performance. The thermal aging test (*T* = 80 °C) (Figure S54) shows that the device based on the poly-alloy HTL remained 93% of its initial efficiency after 600 h in a N₂-filled glovebox, whereas the Spiro-OMeTAD-based device exhibited substantial degradation, which could be ascribed to the severe deterioration at the interface between the perovskite and Spiro-OMeTAD caused by lithium-ion diffusion.⁴⁷ Also, we tested the long-term stability of unencapsulated devices illuminated under continuous 1 sun irradiation (white light LED) at room temperature in N₂ (Figure S55). Under maximum power point (MPP) conditions, the Spiro-OMeTAD-based device dropped to ~56% of its initial PCE after 405 h. By contrast, the poly-alloy HTL-based device sustained over 88% of its original efficiency after 648 h.

CONCLUSIONS

In summary, we have reported a strategy to utilize a polymer alloy as a dopant-free HTL to simultaneously enhance the device efficiency and stability in n-i-p type PSCs. The polymeric packing and crystallinity could be regulated finely via tuning the weight ratio of two conjugated polymers with highly similar structures but different crystallinities. The

optimized PSCs using the poly-alloy HTL without any dopants yield an excellent PCE of 24.53% and a high V_{OC} of 1.9 V. Importantly, the device could maintain 96% of their initial efficiency after 1200 h in air (relative humidity, RH = 30 ± 5%) owing to its dopant-free properties and much better hydrophobicity than that of doped spiro-OMeTAD. The universality of our polymer alloy strategy has been further verified by its applicability in different perovskite systems. We firmly believe that our strategy via polymer alloying will open a new avenue for the design of dopant-free HTMs for highly efficient and stable PSCs and promote the commercialization of this technology.

■ ASSOCIATED CONTENT

SI Supporting Information

The Supporting Information is available free of charge at <https://pubs.acs.org/doi/10.1021/jacs.2c04029>.

Material synthesis; GPC; device characterization and stability measurements; charge mobility; theoretical calculations; and ^1H NMR and ^{13}C NMR data (PDF)

■ AUTHOR INFORMATION

Corresponding Authors

Yongsheng Chen – *The Centre of Nanoscale Science and Technology and Key Laboratory of Functional Polymer Materials, Institute of Polymer Chemistry, College of Chemistry and Renewable Energy Conversion and Storage Center (RECAST), Nankai University, Tianjin 300071, China; Haihe Laboratory of Sustainable Chemical Transformations, Tianjin 300192, China; orcid.org/0000-0003-1448-8177; Email: yschen99@nankai.edu.cn*

Yongsheng Liu – *The Centre of Nanoscale Science and Technology and Key Laboratory of Functional Polymer Materials, Institute of Polymer Chemistry, College of Chemistry and Renewable Energy Conversion and Storage Center (RECAST), Nankai University, Tianjin 300071, China; Haihe Laboratory of Sustainable Chemical Transformations, Tianjin 300192, China; orcid.org/0000-0002-7135-723X; Email: liuys@nankai.edu.cn*

Authors

Qiang Fu – *The Centre of Nanoscale Science and Technology and Key Laboratory of Functional Polymer Materials, Institute of Polymer Chemistry, College of Chemistry and Renewable Energy Conversion and Storage Center (RECAST), Nankai University, Tianjin 300071, China*

Xingchen Tang – *The Centre of Nanoscale Science and Technology and Key Laboratory of Functional Polymer Materials, Institute of Polymer Chemistry, College of Chemistry and Renewable Energy Conversion and Storage Center (RECAST), Nankai University, Tianjin 300071, China*

Hang Liu – *The Centre of Nanoscale Science and Technology and Key Laboratory of Functional Polymer Materials, Institute of Polymer Chemistry, College of Chemistry and Renewable Energy Conversion and Storage Center (RECAST), Nankai University, Tianjin 300071, China*

Rui Wang – *The Centre of Nanoscale Science and Technology and Key Laboratory of Functional Polymer Materials, Institute of Polymer Chemistry, College of Chemistry and Renewable Energy Conversion and Storage Center (RECAST), Nankai University, Tianjin 300071, China*

Tingting Liu – *The Centre of Nanoscale Science and Technology and Key Laboratory of Functional Polymer Materials, Institute of Polymer Chemistry, College of Chemistry and Renewable Energy Conversion and Storage Center (RECAST), Nankai University, Tianjin 300071, China*

Ziang Wu – *Department of Chemistry, Korea University, Seoul 02841, South Korea*

Han Young Woo – *Department of Chemistry, Korea University, Seoul 02841, South Korea; orcid.org/0000-0001-5650-7482*

Tong Zhou – *The Centre of Nanoscale Science and Technology and Key Laboratory of Functional Polymer Materials, Institute of Polymer Chemistry, College of Chemistry and Renewable Energy Conversion and Storage Center (RECAST), Nankai University, Tianjin 300071, China*

Xiangjian Wan – *The Centre of Nanoscale Science and Technology and Key Laboratory of Functional Polymer Materials, Institute of Polymer Chemistry, College of Chemistry and Renewable Energy Conversion and Storage Center (RECAST), Nankai University, Tianjin 300071, China; Haihe Laboratory of Sustainable Chemical Transformations, Tianjin 300192, China; orcid.org/0000-0001-5266-8510*

Complete contact information is available at:

<https://pubs.acs.org/doi/10.1021/jacs.2c04029>

Notes

The authors declare no competing financial interest.

■ ACKNOWLEDGMENTS

The authors gratefully acknowledge the financial support from the National Key Research and Development Program of China (No. 2019YFA0705900), the National Natural Science Foundation of China (Grants No. 21875122), and the Haihe Laboratory of Sustainable Chemical Transformations.

■ REFERENCES

- (1) Kojima, A.; Teshima, K.; Shirai, Y.; Miyasaka, T. Organometal Halide Perovskites as Visible-Light Sensitizers for Photovoltaic Cells. *J. Am. Chem. Soc.* **2009**, *131*, 6050–6051.
- (2) Kim, H.-S.; Lee, C.-R.; Im, J.-H.; Lee, K.-B.; Moehl, T.; Marchioro, A.; Moon, S.-J.; Humphry-Baker, R.; Yum, J.-H.; Moser, J. E.; Grätzel, M.; Park, N.-G. Lead Iodide Perovskite Sensitized All-Solid-State Submicron Thin Film Mesoscopic Solar Cell with Efficiency Exceeding 9%. *Sci. Rep.* **2012**, *2*, No. 591.
- (3) Lee, M. M.; Teuscher, J.; Miyasaka, T.; Murakami, T. N.; Snaith, H. J. Efficient Hybrid Solar Cells Based on Meso-Superstructured Organometal Halide Perovskites. *Science* **2012**, *338*, 643–647.
- (4) Zhou, H.; Chen, Q.; Li, G.; Luo, S.; Song, T.-b.; Duan, H.-S.; Hong, Z.; You, J.; Liu, Y.; Yang, Y. Interface engineering of highly efficient perovskite solar cells. *Science* **2014**, *345*, 542–546.
- (5) Luo, D.; Yang, W.; Wang, Z.; Sadhanala, A.; Hu, Q.; Su, R.; Shivanna, R.; Trindade, G. F.; Watts, J. F.; Xu, Z.; Liu, T.; Chen, K.; Ye, F.; Wu, P.; Zhao, L.; Wu, J.; Tu, Y.; Zhang, Y.; Yang, X.; Zhang, W.; Friend, R. H.; Gong, Q.; Snaith, H. J.; Zhu, R. Enhanced photovoltage for inverted planar heterojunction perovskite solar cells. *Science* **2018**, *360*, 1442–1446.
- (6) Jiang, Q.; Zhao, Y.; Zhang, X.; Yang, X.; Chen, Y.; Chu, Z.; Ye, Q.; Li, X.; Yin, Z.; You, J. Surface passivation of perovskite film for efficient solar cells. *Nat. Photonics* **2019**, *13*, 460–466.
- (7) Kim, J. Y.; Lee, J.-W.; Jung, H. S.; Shin, H.; Park, N.-G. High-Efficiency Perovskite Solar Cells. *Chem. Rev.* **2020**, *120*, 7867–7918.

- (8) Kim, G.; Min, H.; Lee, K. S.; Lee, D. Y.; Yoon, S. M.; Seok, S. I. Impact of strain relaxation on performance of α -formamidinium lead iodide perovskite solar cells. *Science* **2020**, *370*, 108–112.
- (9) National Renewable Energy Laboratory Efficiency Chart. <https://www.nrel.gov/pv/cell-efficiency.html> (accessed December, 2021).
- (10) Schloemer, T. H.; Christians, J. A.; Luther, J. M.; Sellinger, A. Doping strategies for small molecule organic hole-transport materials: impacts on perovskite solar cell performance and stability. *Chem. Sci.* **2019**, *10*, 1904–1935.
- (11) Desoky, M. M. H.; Bonomo, M.; Barbero, N.; Viscardi, G.; Barolo, C.; Quagliotto, P. Polymeric Dopant-Free Hole Transporting Materials for Perovskite Solar Cells: Structures and Concepts towards Better Performances. *Polymers* **2021**, *13*, No. 1652.
- (12) Noh, J. H.; Jeon, N. J.; Choi, Y. C.; Nazeeruddin, M. K.; Grätzel, M.; Seok, S. I. Nanostructured TiO₂/CH₃NH₃PbI₃ heterojunction solar cells employing spiro-OMeTAD/Co-complex as hole-transporting material. *J. Mater. Chem. A* **2013**, *1*, 11842–11847.
- (13) Juarez-Perez, E. J.; Leyden, M. R.; Wang, S.; Ono, L. K.; Hawash, Z.; Qi, Y. Role of the Dopants on the Morphological and Transport Properties of Spiro-MeOTAD Hole Transport Layer. *Chem. Mater.* **2016**, *28*, 5702–5709.
- (14) Jeong, M.; Choi, I. W.; Go, E. M.; Cho, Y.; Kim, M.; Lee, B.; Jeong, S.; Jo, Y.; Choi, H. W.; Lee, J.; Bae, J.-H.; Kwak, S. K.; Kim, D. S.; Yang, C. Stable perovskite solar cells with efficiency exceeding 24.8% and 0.3-V voltage loss. *Science* **2020**, *369*, 1615–1620.
- (15) Kim, G.-W.; Choi, H.; Kim, M.; Lee, J.; Son, S. Y.; Park, T. Hole Transport Materials in Conventional Structural (n-i-p) Perovskite Solar Cells: From Past to the Future. *Adv. Energy Mater.* **2020**, *10*, No. 1903403.
- (16) Pham, H. D.; Yang, T. C.-J.; Jain, S. M.; Wilson, G. J.; Sonar, P. Development of Dopant-Free Organic Hole Transporting Materials for Perovskite Solar Cells. *Adv. Energy Mater.* **2020**, *10*, No. 1903326.
- (17) Zhao, B. X.; Yao, C.; Gu, K.; Liu, T.; Xia, Y.; Loo, Y.-L. A hole-transport material that also passivates perovskite surface defects for solar cells with improved efficiency and stability. *Energy Environ. Sci.* **2020**, *13*, 4334–4343.
- (18) Guo, H.; Zhang, H.; Shen, C.; Zhang, D.; Liu, S.; Wu, Y.; Zhu, W.-H. A Coplanar π -Extended Quinoxaline Based Hole-Transporting Material Enabling over 21% Efficiency for Dopant-Free Perovskite Solar Cells. *Angew. Chem., Int. Ed.* **2021**, *60*, 2674–2679.
- (19) Lee, J.; Kim, G.-W.; Kim, M.; Park, S. A.; Park, T. Nonaromatic Green-Solvent-Processable, Dopant-Free, and Lead-Capturable Hole Transport Polymers in Perovskite Solar Cells with High Efficiency. *Adv. Energy Mater.* **2020**, *10*, No. 1902662.
- (20) Yao, Z.; Zhang, F.; Guo, Y.; Wu, H.; He, L.; Liu, Z.; Cai, B.; Guo, Y.; Brett, C. J.; Li, Y.; Srmbickal, C. V.; Yang, X.; Chen, G.; Widengren, J.; Liu, D.; Gardner, J. M.; Kloos, L.; Sun, L. Conformational and Compositional Tuning of Phenanthrocarbazole-Based Dopant-Free Hole-Transport Polymers Boosting the Performance of Perovskite Solar Cells. *J. Am. Chem. Soc.* **2020**, *142*, 17681–17692.
- (21) Jeong, J.; Kim, M.; Seo, J.; Lu, H.; Ahlawat, P.; Mishra, A.; Yang, Y.; Hope, M. A.; Eickemeyer, F. T.; Kim, M.; Yoon, Y. J.; Choi, I. W.; Darwich, B. P.; Choi, S. J.; Jo, Y.; Lee, J. H.; Walker, B.; Zakeeruddin, S. M.; Emmsley, L.; Rothlisberger, U.; Hagfeldt, A.; Kim, D. S.; Grätzel, M.; Kim, J. Y. Pseudo-halide anion engineering for α -FAPbI₃ perovskite solar cells. *Nature* **2021**, *592*, 381–385.
- (22) Jung, E. H.; Jeon, N. J.; Park, E. Y.; Moon, C. S.; Shin, T. J.; Yang, T.-Y.; Noh, J. H.; Seo, J. Efficient, stable and scalable perovskite solar cells using poly(3-hexylthiophene). *Nature* **2019**, *567*, 511–515.
- (23) Fu, Q.; Xu, Z.; Tang, X.; Liu, T.; Dong, X.; Zhang, X.; Zheng, N.; Xie, Z.; Liu, Y. Multifunctional Two-Dimensional Conjugated Materials for Dopant-Free Perovskite Solar Cells with Efficiency Exceeding 22%. *ACS Energy Lett.* **2021**, *6*, 1521–1532.
- (24) Wang, Y.; Liao, Q.; Chen, J.; Huang, W.; Zhuang, X.; Tang, Y.; Li, B.; Yao, X.; Feng, X.; Zhang, X.; Su, M.; He, Z.; Marks, T. J.; Facchetti, A.; Guo, X. Teaching an Old Anchoring Group New Tricks: Enabling Low-Cost, Eco-Friendly Hole-Transporting Materials for Efficient and Stable Perovskite Solar Cells. *J. Am. Chem. Soc.* **2020**, *142*, 16632–16643.
- (25) Zhao, W.; Li, S.; Yao, H.; Zhang, S.; Zhang, Y.; Yang, B.; Hou, J. Molecular Optimization Enables over 13% Efficiency in Organic Solar Cells. *J. Am. Chem. Soc.* **2017**, *139*, 7148–7151.
- (26) Nadkarni, V. M. Polymer alloys: science and practice. *Proc. Indian Acad. Sci.* **1983**, *92*, 623–637.
- (27) Shen, W.; Chen, W.; Zhu, D.; Zhang, J.; Xu, X.; Jiang, H.; Wang, T.; Wang, E.; Yang, R. High-performance ternary polymer solar cells from a structurally similar polymer alloy. *J. Mater. Chem. A* **2017**, *5*, 12400–12406.
- (28) Zhou, Z.; Wu, Q.; Cheng, R.; Zhang, H.; Wang, S.; Chen, M.; Xie, M.; Chan, P. K. L.; Grätzel, M.; Feng, S.-P. Orientation-Engineered Small-Molecule Semiconductors as Dopant-Free Hole Transporting Materials for Efficient and Stable Perovskite Solar Cells. *Adv. Funct. Mater.* **2021**, *31*, No. 2011270.
- (29) Sun, X.; Yu, X.; Li, Z. Recent Advances of Dopant-Free Polymer Hole-Transporting Materials for Perovskite Solar Cells. *ACS Appl. Energy Mater.* **2020**, *3*, 10282–10302.
- (30) Fan, Q.; Fu, H.; Wu, Q.; Wu, Z.; Lin, F.; Zhu, Z.; Min, J.; Woo, H. Y.; Jen, A. K. Y. Multi-Selenophene-Containing Narrow Bandgap Polymer Acceptors for All-Polymer Solar Cells with over 15% Efficiency and High Reproducibility. *Angew. Chem., Int. Ed.* **2021**, *60*, 15935–15943.
- (31) Wang, J.; Wu, X.; Liu, Y.; Qin, T.; Zhang, K.; Li, N.; Zhao, J.; Ye, R.; Fan, Z.; Chi, Z.; Zhu, Z. Dopant-Free Hole-Transporting Material with Enhanced Intermolecular Interaction for Efficient and Stable n-i-p Perovskite Solar Cells. *Adv. Energy Mater.* **2021**, *11*, No. 2100967.
- (32) Fu, Q.; Wang, T.; Sun, Y.; Zheng, N.; Xie, Z.; Lu, D.; Xu, Z.; Wan, X.; Zhang, Y.; Liu, Y. A solution-processed nanoscale COF-like material towards optoelectronic applications. *Sci. China: Chem.* **2021**, *64*, 82–91.
- (33) Ashraf, R. S.; Meager, I.; Nikolka, M.; Kirkus, M.; Planells, M.; Schroeder, B. C.; Holliday, S.; Hurhangee, M.; Nielsen, C. B.; Sirringhaus, H.; McCulloch, I. Chalcogenophene Comonomer Comparison in Small Band Gap Diketopyrrolopyrrole-Based Conjugated Polymers for High-Performing Field-Effect Transistors and Organic Solar Cells. *J. Am. Chem. Soc.* **2015**, *137*, 1314–1321.
- (34) Oh, S.; Song, C. E.; Lee, T.; Cho, A.; Lee, H. K.; Lee, J.-C.; Moon, S.-J.; Lim, E.; Lee, S. K.; Shin, W. S. Enhanced efficiency and stability of PTB7-Th-based multi-non-fullerene solar cells enabled by the working mechanism of the coexisting alloy-like structure and energy transfer model. *J. Mater. Chem. A* **2019**, *7*, 22044–22053.
- (35) Mai, C.-L.; Zhou, Q.; Xiong, Q.; Chen, C.-C.; Xu, J.; Zhang, Z.; Lee, H.-W.; Yeh, C.-Y.; Gao, P. Donor- π -Acceptor Type Porphyrin Derivatives Assisted Defect Passivation for Efficient Hybrid Perovskite Solar Cells. *Adv. Funct. Mater.* **2021**, *31*, No. 2007762.
- (36) Wang, S.; Chen, H.; Zhang, J.; Xu, G.; Chen, W.; Xue, R.; Zhang, M.; Li, Y.; Li, Y. Targeted Therapy for Interfacial Engineering Toward Stable and Efficient Perovskite Solar Cells. *Adv. Mater.* **2019**, *31*, No. 1903691.
- (37) Zhou, K.; Wu, Y.; Liu, Y.; Zhou, X.; Zhang, L.; Ma, W. Molecular Orientation of Polymer Acceptor Dominates Open-Circuit Voltage Losses in All-Polymer Solar Cells. *ACS Energy Lett.* **2019**, *4*, 1057–1064.
- (38) Hu, Q.; Chen, W.; Yang, W.; Li, Y.; Zhou, Y.; Larson, B. W.; Johnson, J. C.; Lu, Y.-H.; Zhong, W.; Xu, J.; Klivansky, L.; Wang, C.; Salmeron, M.; Djurišić, A. B.; Liu, F.; He, Z.; Zhu, R.; Russell, T. P. Improving Efficiency and Stability of Perovskite Solar Cells Enabled by a Near-Infrared-Absorbing Moisture Barrier. *Joule* **2020**, *4*, 1575–1593.
- (39) Wang, R.; Xue, J.; Wang, K.-L.; Wang, Z.-K.; Luo, Y.; Fenning, D.; Xu, G.; Nuryyeva, S.; Huang, T.; Zhao, Y.; Yang Jonathan, L.; Zhu, J.; Wang, M.; Tan, S.; Yavuz, I.; Houk Kendall, N.; Yang, Y. Constructive molecular configurations for surface-defect passivation of perovskite photovoltaics. *Science* **2019**, *366*, 1509–1513.

(40) Zhao, D. W.; Liu, P.; Sun, X. W.; Tan, S. T.; Ke, L.; Kyaw, A. K. An inverted organic solar cell with an ultrathin Ca electron-transporting layer and MoO₃ hole-transporting layer. *Appl. Phys. Lett.* **2009**, *95*, No. 153304.

(41) Liu, Y.; Hong, Z.; Chen, Q.; Chen, H.; Chang, W.-H.; Yang, Y.; Song, T.-B.; Yang, Y. Perovskite Solar Cells Employing Dopant-Free Organic Hole Transport Materials with Tunable Energy Levels. *Adv. Mater.* **2016**, *28*, 440–446.

(42) Hou, Y.; Du, X.; Scheiner, S.; McMeekin David, P.; Wang, Z.; Li, N.; Killian Manuela, S.; Chen, H.; Richter, M.; Levchuk, I.; Schrenker, N.; Spiecker, E.; Stubhan, T.; Luechinger Norman, A.; Hirsch, A.; Schmuki, P.; Steinrück, H.-P.; Fink Rainer, H.; Halik, M.; Snaith Henry, J.; Brabec Christoph, J. A generic interface to reduce the efficiency-stability-cost gap of perovskite solar cells. *Science* **2017**, *358*, 1192–1197.

(43) Almora, O.; Aranda, C.; Mas-Marzá, E.; Garcia-Belmonte, G. On Mott-Schottky analysis interpretation of capacitance measurements in organometal perovskite solar cells. *Appl. Phys. Lett.* **2016**, *109*, No. 173903.

(44) Yoo, J. J.; Wieghold, S.; Sponseller, M. C.; Chua, M. R.; Bertram, S. N.; Hartono, N. T. P.; Tresback, J. S.; Hansen, E. C.; Correa-Baena, J.-P.; Bulović, V.; Buonassisi, T.; Shin, S. S.; Bawendi, M. G. An interface stabilized perovskite solar cell with high stabilized efficiency and low voltage loss. *Energy Environ. Sci.* **2019**, *12*, 2192–2199.

(45) Tress, W.; Marinova, N.; Inganäs, O.; Nazeeruddin, M. K.; Zakeeruddin, S. M.; Graetzel, M. Predicting the Open-Circuit Voltage of CH₃NH₃PbI₃ Perovskite Solar Cells Using Electroluminescence and Photovoltaic Quantum Efficiency Spectra: the Role of Radiative and Non-Radiative Recombination. *Adv. Energy Mater.* **2015**, *5*, No. 1400812.

(46) Yang, G.; Ren, Z.; Liu, K.; Qin, M.; Deng, W.; Zhang, H.; Wang, H.; Liang, J.; Ye, F.; Liang, Q.; Yin, H.; Chen, Y.; Zhuang, Y.; Li, S.; Gao, B.; Wang, J.; Shi, T.; Wang, X.; Lu, X.; Wu, H.; Hou, J.; Lei, D.; So, S. K.; Yang, Y.; Fang, G.; Li, G. Stable and low-photovoltage-loss perovskite solar cells by multifunctional passivation. *Nat. Photonics* **2021**, *15*, 681–689.

(47) Jena, A. K.; Ikegami, M.; Miyasaka, T. Severe Morphological Deformation of Spiro-OMeTAD in (CH₃NH₃)PbI₃ Solar Cells at High Temperature. *ACS Energy Lett.* **2017**, *2*, 1760–1761.

Recommended by ACS

Improving the Fill Factor of Perovskite Solar Cells by Employing an Amine-tethered Diketopyrrolopyrrole-Based Polymer as the Dopant-free Hole Transport Layer

Wenbo Liu, Qichun Zhang, *et al.*

SEPTEMBER 11, 2020
ACS APPLIED ENERGY MATERIALS

READ 

Recent Advances of Dopant-Free Polymer Hole-Transporting Materials for Perovskite Solar Cells

Xianglang Sun, Zhong'an Li, *et al.*

OCTOBER 28, 2020
ACS APPLIED ENERGY MATERIALS

READ 

Polymeric, Cost-Effective, Dopant-Free Hole Transport Materials for Efficient and Stable Perovskite Solar Cells

Fuguo Zhang, Licheng Sun, *et al.*

NOVEMBER 20, 2019
JOURNAL OF THE AMERICAN CHEMICAL SOCIETY

READ 

Molecular Engineering of Polymeric Hole-Transporting Materials for Efficient and Stable Perovskite Solar Cells

Yan Li, Baomin Xu, *et al.*

APRIL 07, 2021
ACS APPLIED ENERGY MATERIALS

READ 

Get More Suggestions >